J Inorg Organomet Polym (2017) 27:266–274
DOI 10.1007/s10904-016-0469-5

Characterization of Diatomite Platelets and Its Application for In Situ Atom Transfer Radical Random Copolymerization of Styrene and Butyl Acrylate: Normal Approach

Khezrollah Khezri[1] · **Yousef Fazli**[2]

Received: 31 July 2016 / Accepted: 7 November 2016 / Published online: 22 November 2016

Abstract Pristine mesoporous diatomite platelets were employed to prepare poly(styrene-co-butyl acrylate)/diatomite composites. Diatomite platelets were used for in situ copolymerization of styrene and butyl acrylate by ATRP to synthesize tailor-made poly(styrene-co-butyl acrylate) nanocomposites. XRF analysis, FTIR spectroscopy, TGA, nitrogen adsorption/desorption isotherm, SEM, and TEM were employed for evaluating inherent properties of pristine diatomite nanoplatelets. Conversion and molecular weight determinations were performed using GC and SEC respectively. Addition of 3 wt% pristine mesoporous diatomite platelets leads to increase of conversion from 65 to 78%. Molecular weight of copolymer chains increases from 15,500 to 19,000 by addition of 3 wt% pristine mesoporous diatomite; however, dispersity increases from 1.1 to 1.4. Copolymers composition was evaluated using ^{1}H NMR spectroscopy. Increasing thermal stability of the nanocomposites is demonstrated by TGA. DSC shows an increase in glass transition temperature from 34.6 to 38.8 °C by adding 3 wt% of mesoporous diatomite platelets.

Keywords Mesoporous diatomite platelets · Nanocomposite · Poly(styrene-co-butyl acrylate) · In situ ATRP

✉ Yousef Fazli
y-fazli@iau-arak.ac.ir; yousef.fazli75@gmail.com

[1] Young Researchers and Elites Club, Central Tehran Branch, Islamic Azad University, Tehran, Iran

[2] Department of Chemistry, Faculty of Science, Arak Branch, Islamic Azad University, Arak, Iran

1 Introduction

During the last decades, the utility of inorganic nano-materials as additives to enhance polymer performance has been established and opened interesting opportunities for many diverse applications [1, 2]. Nanocomposites originate from suitable dispersion of nano-materials or nanosized objects within polymer matrix in which results in materials with unique properties [3]. Nano-materials have a large surface area for a given volume and therefore low-volume addition of them can lead to substantial enhancements in mechanical, thermal, and barrier properties relative to those of the unfilled or conventionally filled polymer [4, 5]. Polymer nanocomposites can combine the unique advantages of organic (e.g. dielectric, ductility and processability) and inorganic parts (e.g. rigidity and thermal stability) [6]. Depending on the shape of the nano-filler, nanocomposites can be classified into three main groups: Nanoparticles (with three-dimensional nanosize distribution), nanotubes or whiskers (with two-dimensional nanosize distribution), and phyllosilicates such as nanoclay (with one-dimensional nanosize distribution) [7]. The pathways for synthesis and preparation of polymer based nanocomposites include melt intercalation, solution and in situ. In the in situ polymerization, the monomer is directly faced with the nano-filler and subsequently polymerization takes place [8].

Diatomite is pale-colored, soft, and lightweight sedimentary rock that is composed generally of silica microfossils of aquatic unicellular algae. Diatomite is generally consisted of silicon dioxide (SiO_2) and considerable amounts of Al_2O_3 and Fe_2O_3. The structure of diatomite contains up to 80% voids with various diameters. Since diatomite platelets are mainly composed of hydrated silica ($SiO_2{\cdot}nH_2O$), they are classified as noncrystalline opal-A (in mineralogical classification) [9–12]. Diatomite presents

unique features such as highly porous structure, high silica content, low density, large surface area, and low conductivity coefficient [9, 13]. The unique combination of physical and chemical properties of diatomite, make it applicable for many diverse applications. Support in the reactions, sound and heat insulation, water treatment, removal processes, and manufacture of explosives and as filters are some examples for various applications of diatomite [9, 14, 15].

Production of over 50% of all the polymeric materials by free radical polymerization (FRP) is a powerful evidence for industrial utility of this method [16]. Polymerization of various monomers, large range of reaction temperature (−100 to >200 °C), application for different polymerization systems and media are some advantageous characters of FRP. Although FRP provides numerous advantages over other polymerization methods, it can not be applied to synthesize pure block copolymer and tailor-made polymers with predetermined molecular weight and low dispersity [16, 17]. Synthesis of polymers with tailor-made composition, architectures, and functionalities was a long-standing goal for polymer chemists. Introducing controlled/living radical polymerization (CRP) has opened an appropriate pathway to synthesize tailor-made (co)polymers with favorite features [18–20]. By using CRP, synthesis of pure block copolymers, polymers with predetermined Mw, polymers with low dispersity values, and various polymers with desired composition, architectures, and functionalities can be obtained. CRP is classified into three main methods: atom transfer radical polymerization (ATRP), nitroxide-mediated polymerization (NMP), and reversible addition fragmentation chain transfer (RAFT) [21–23]. Compared with other CRP methods, ATRP provides a simple route to prepare polymers with well-defined chain end-functionalities and complex architectures [24]. Polymerization of wide variety of monomers, commercial availability of its reagents, and application for different polymerization systems and media are other interesting properties of ATRP over other CRP methods [24, 25]. Tailor-made organic polymers with desired composition, architecture, end-functionalities, and predetermined Mw can interestingly participate in the preparation of nanocomposites and therefore application of CRP in the field of nanocomposites has attracted great attention during the last decade [26].

A review of literatures indicates that application of diatomite as filler to synthesize polymer/diatomite composites have attracted considerable attention. Karaman et al. have prepared polyethylene glycol (PEG)/diatomite composite as a novel form-stable composite phase change material (PCM) in which the PCM was prepared by incorporating PEG in the pores of diatomite [27]. Li et al. have synthesized conducting composite by polyaniline on the surface of diatomite. Linkage of polyaniline on the surface of diatomite is attributed to the hydrogen bond between the surface of diatomite and polyaniline macromolecules [28]. Li et al. have also prepared fibrillar polyaniline/diatomite composite by one-step in situ polymerization. According to their results, the polyaniline/diatomite composite can be applied as fillers for electromagnetic shielding materials and conductive coatings [29]. In addition, other studies such as investigating the effects of extrusion conditions on die-swell behavior of polypropylene/diatomite composite melts and Crystallization behaviors and foaming properties of diatomite-filled polypropylene composites have been performed [30, 31].

In this research, we take unique advantages of normal ATRP method to synthesize well-defined random poly(styrene-co-butyl acrylate) nanocomposites. The ATRP process was applied to the mixture of monomer and pristine diatomite nanoplatelets to prepare well-defined nanocomposite using in situ polymerization procedure. We have tried to investigate the effect of diatomite loading on the kinetics parameters of the polymerization, thermal stability, and glass transition temperature of the products.

2 Experimental

2.1 Materials

Diatomite earth sample was obtained from Kamel Abad-Azerbaijan-I.R. Iran. It was dispersed in 100 ml distilled water by magnetic stirring and then it was kept constant until some solid impurities were dispersed. The particles were separated with filter paper and dried at 100 °C for 8 h. Styrene (St, Aldrich, 99%) and butyl acrylate (BA, Merck, 99%) were passed through an alumina-filled column, dried over calcium hydride, and distilled under reduced pressure (60 °C, 40 mm Hg). Copper(I) bromide (CuBr, Aldrich, 98%) was washed with glacial acetic acid, filtered, and finally washed with ethanol; it was dried in a vacuum oven (50 °C, 40 mmHg) and then stored in a nitrogen atmosphere. *N,N,N′,N″,N″*-pentamethyldiethylenetriamine (PMDETA, Aldrich, 99%), ethyl alpha-bromoisobutyrate (EBiB, Aldrich, 97%), anisole (Aldrich, 99%), tetrahydrofuran (THF, Merck, 99%), and neutral aluminum oxide (Aldrich, 99%) were used as received.

2.2 Synthesis of Pure Random Poly(styrene-co-butyl acrylate) and Its Different Nanocomposites Via Normal ATRP

Normal atom transfer radical random copolymerization of styrene and butyl acrylate was performed in a 150-ml three-neck lab reactor equipped with a reflux condenser, nitrogen inlet valve, and a magnetic stir bar that was placed in an oil bath. A typical batch of copolymerization

was run at 100 °C with the molar ratio of 200:1:1:1 for $[M]_0$:$[EBiB]_0$:$[CuBr]_0$:$[PMDETA]_0$ giving a theoretical copolymer molecular weight of 23,232 at 100% conversion. At first, styrene (13.34 ml, 0.11 mol), butyl acrylate (8.33 ml. 0.05 mol), CuBr (0.125 g, 0.87 mmol), PMDETA (0.18 ml, 0.87 mmol) and anisole (10 ml) were added to the reactor. Then, it was degassed and back-filled with nitrogen three times, and then left under N_2 with stirring at room temperature. The solution turned light green as the CuBr/PMDETA complex was formed. When the majority of the metal complex had formed, reaction temperature was increased to 100 °C during 5 min. Subsequently, ATRP initiator (EBiB, 0.12 mL, 0.87 mmol) was injected into the reactor to start the styrene normal ATRP. Samples were taken at the end of the reaction (12 h) to measure the final conversion. For preparation of nanocomposites, a desired amount of pristine diatomite nanoplatelets was dispersed in 8 ml of styrene and the mixture was stirred for 23 h. Then, the remained 5.34 ml of styrene was added to the mixture. Subsequently, copolymerization procedure was applied accordingly. In the samples designation, PPSB refers to the neat random poly(styrene-co-butyl acrylate) and PSBD X implies different nanocomposites with X percentages of pristine diatomite content.

2.3 Separation of Copolymer Chains from Pristine Diatomite Nanoplatelets and Catalyst Removal

For separation of poly(styrene-co-butyl acrylate) chains from pristine diatomite particles, nanocomposites were dissolved in THF. By high-speed ultracentrifugation (10,000 rpm) and then passing the solution through a 0.2 μm filter, poly(styrene-co-butyl acrylate) chains were separated from pristine diatomite particles. Subsequently, copolymer solutions passed through an alumina column to remove catalyst species.

2.4 Characterization

Characterization of the pristine diatomite sample for its chemical composition was performed by X-ray fluorescence spectrometer (XRF, Philips 2400). FTIR spectrum of the pristine diatomite was achieved using FTIR spectroscopy on a Bruker FTIR spectrophotometer, within a range of 400–4400 cm^{-1}. Materials porosity was characterized by N_2 adsorption/desorption curves obtained with a Quntasurb QS18 (Quntachrom) apparatus. The surface area and pore size distribution values were obtained with the corrected BET equation (Brunauer–Emmett–Teller). In addition, specific surface area measurements were also performed with NS-93 apparatus (Towse-e-Hesgarsazan Asia, Iran). Surface morphology of the pristine diatomite was examined by scanning electron microscope (SEM, Philips XL30 and LEO-1455VP) with acceleration voltage of 20 kV. The transmission electron microscope (TEM), Philips EM 208 (The Netherlands), with an accelerating voltage of 120 kV was employed to study the morphology of the pristine diatomite sample. The specimens were prepared by coating a thin layer on a mica surface using a spin coater (Modern Technology Development Institute, Iran). Gas chromatography (GC) is a simple and highly sensitive characterization method and does not require removal of the metal catalyst particles. GC was performed on an Agilent-6890N with a split/splitless injector and flame ionization detector, using a 60 m HP-INNOWAX capillary column for the separation. The GC temperature profile included an initial steady heating at 60 °C for 10 min and a 10 °C min^{-1} ramp from 60 to 160 °C. The samples were also diluted with acetone. The ratio of monomer to anisole was measured by GC to calculate monomer conversion throughout the reaction. Size exclusion chromatography (SEC) was used to measure the molecular weight and molecular weight distribution. A Waters 2000 ALLIANCE with a set of three columns of pore sizes of 10,000, 1000, and 500 Å was utilized to determine polymer average molecular weight and dispersity. THF was used as the eluent at a flow rate of 1.0 mL min^{-1}, and calibration was carried out using low dispersity polystyrene standards. Proton nuclear magnetic resonance spectroscopy (^{1}H NMR) spectra were recorded on a Bruker 300-MHz ^{1}H NMR instrument with $CDCl_3$ as the solvent and tetramethylsilane as the internal standard. Thermal gravimetric analysis (TGA) was carried out with a PL thermo-gravimetric analyzer (Polymer Laboratories, TGA 1000, UK). Thermograms were obtained from ambient temperature to 700 °C at a heating rate of 10 °C min^{-1}. Thermal analysis were carried out using a differential scanning calorimetry (DSC) instrument (NETZSCH DSC 200 F3, Netzsch Co, Selb/Bavaria, Germany). Nitrogen at a rate of 50 mL min^{-1} was used as purging gas. Aluminum pans containing 2–3 mg of the samples were sealed using DSC sample press. The samples were heated from ambient temperature to 225 °C at a heating rate of 10 °C min^{-1}.

3 Results and Discussion

Kinetics of in situ (co)polymerization and consequently nanocomposite properties can be affected from inherent characteristics of the nano-filler or the type of organic modifier on the surface of them [32]. Therefore, morphological studies and evaluation of structural properties of the nano-filler can be considered as a key factor in the synthesis of various nanocomposites.

Table 1 presents the chemical composition of the pristine diatomite that is evaluated by X-ray fluorescence (XRF) technique. According to the results, silica (SiO_2) is

Table 1 The results of XRF analysis

Element	SiO_2	Al_2O_3	CaO	Fe_2O_3	K_2O	MgO	Na_2O	P_2O_5	TiO_2	LOI
Amount (%)	63	13	2.1	5.6	2	1.9	1.9	0.1	0.4	9.4

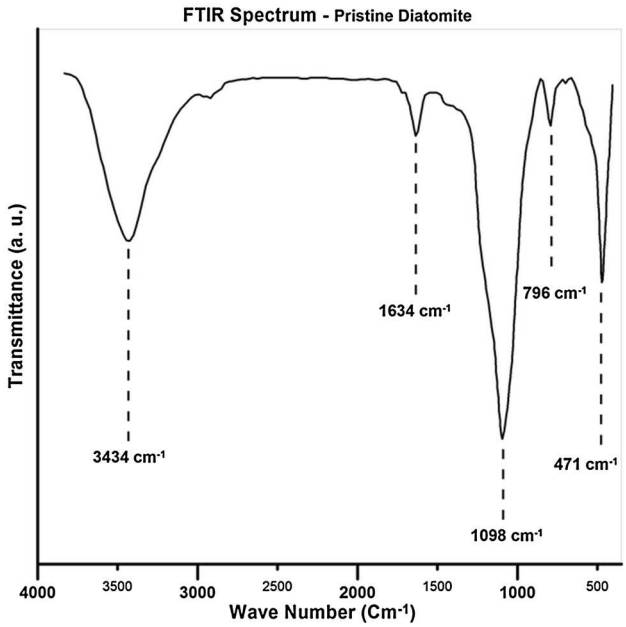

Fig. 1 FTIR spectrum of the pristine diatomite nanoparticles

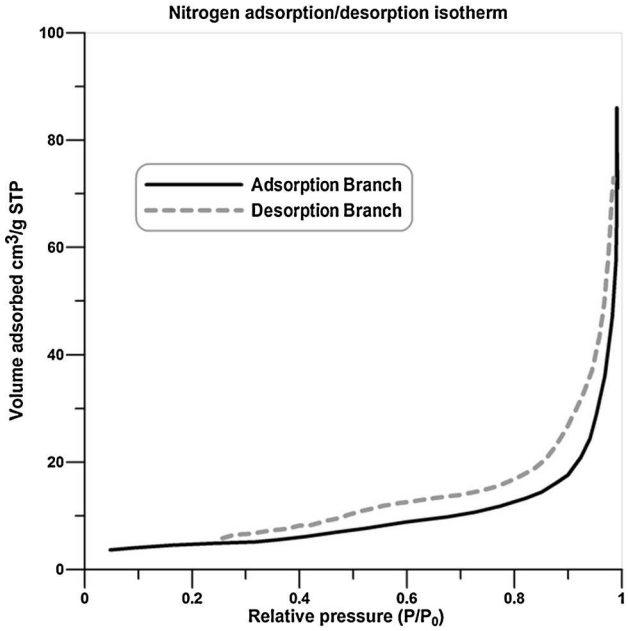

Fig. 2 Nitrogen adsorption/desorption isotherm of the pristine diatomite nanoparticles

the main constituent of the pristine diatomite sample (about 63%). Al_2O_3 is another important constituent of the sample (about 13%). In addition, other impurities are consisting of Fe_2O_3, CaO, K_2O, Na_2O, and TiO_2.

Figure 1 represents FTIR spectrum of the pristine diatomite nanoplatelets. The peaks at 3434 and 1634 cm^{-1} correspond to the stretching vibrations of physically adsorbed water and zeolitic water, respectively [33]. Although the diatomite sample is rehydrated, during the preparation process and obtaining the spectrum some water molecules may be re-adsorbed [34]. The strong peak at 1098 cm^{-1} is attributed to the stretching mode of siloxane (Si–O–Si). In addition, the peak at 471 cm^{-1} is associated with the asymmetric stretching mode of siloxane bonds. The peak at 796 cm^{-1} is also attributed to the vibration of O–H [35, 36].

Figure 2 displays nitrogen adsorption/desorption isotherms of the pristine diatomite nanoplatelets. The shape of isotherm is relatively similar to the IV type isotherms according to the international union of pure and applied chemistry (IUPAC) classification and confirms that diatomite has mesoporous structure [37, 38]. The hysteresis is associated with the filling and emptying of the mesopores by capillary condensation [39]. A sharp increase in the nitrogen adsorbed quantity near the relative pressure of 1 demonstrates the existence of macropores in the pure diatomite and therefore non-uniform pore size distribution can be comprehended [40].

According to extracted data from the nitrogen adsorption/desorption isotherms, surface area of the pristine diatomite particles is calculated 19.6 $m^2\ g^{-1}$. Also, average pore diameter is estimated around 23.4 nm.

Figure 3 illustrates the result of thermogravimetric analysis (TGA) of the pristine diatomite sample. As it can be seen two main mass losses are resolved in the TGA curve. The first mass loss is mainly ascribed to the dehydration of diatomite and the second weight loss (in the temperature range of 400–700 °C) may be associated with the dehydroxylation of the silanols of diatomite nanoplatelets. Pristine diatomite particles leave 92.3% char at 700 °C.

Figure 4 exhibits SEM images of the pristine diatomite nanoplatelets. As it can be seen, the pristine diatomite is composed of plaque plate particles with spherical pores. These plates have regular pores and sometimes are aggregated. This structure of the diatomite is suitable for the synthesis of various composites and makes it as an appropriate catalyst support.

TEM images can be employed to confirm the observations obtained from SEM images and evaluating the

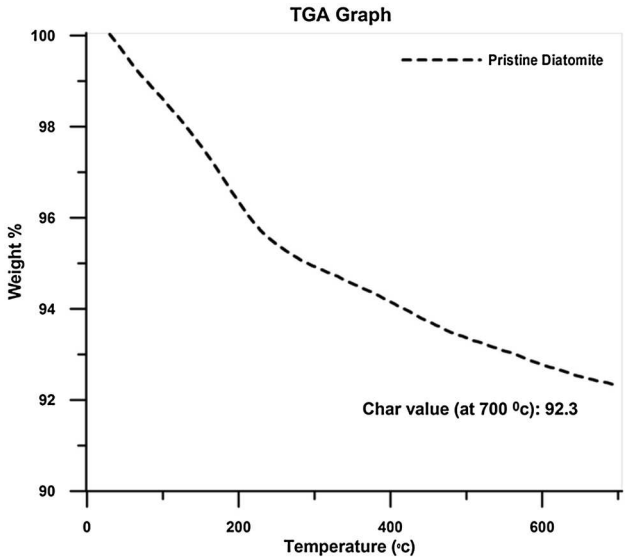

Fig. 3 TGA graph of the pristine diatomite nanoplatelets

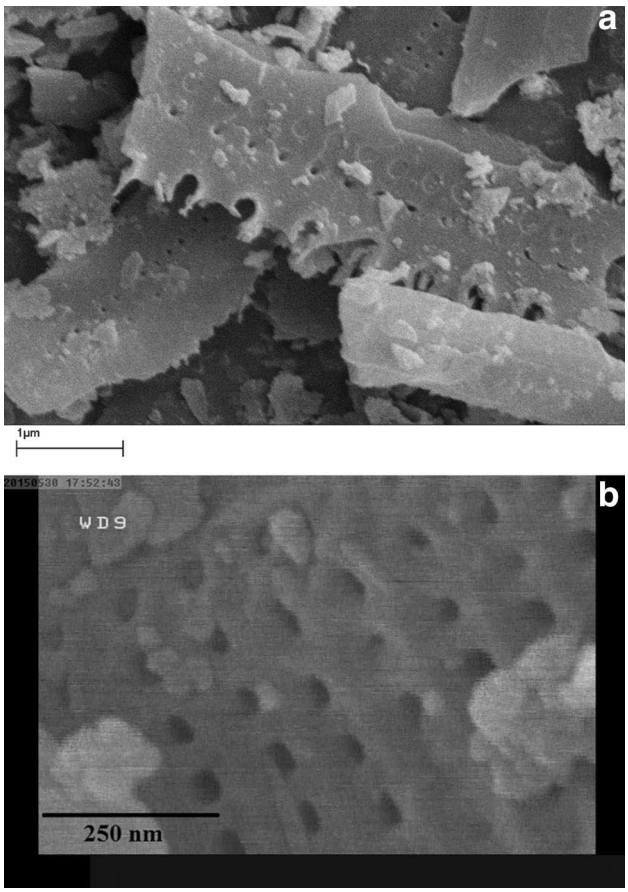

Fig. 4 SEM images (**a** and **b**) of the pristine diatomite nanoplatelets

morphology and pore condition of the pristine diatomite. Figure 5 represents TEM image of the pristine diatomite sample. According to this image, pristine diatomite

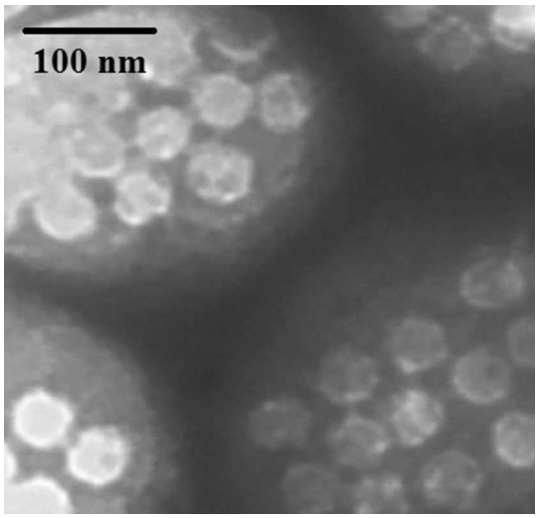

Fig. 5 TEM image of the pristine diatomite nanoplatelets

sample belongs numerous regularly spaced rows of pores in its structure that this observation is confirmed with SEM images. In addition, average pore diameter from TEM images is estimated around 40 nm.

Pristine diatomite nanoplatelets are employed to synthesize tailor-made random poly(styrene-co-butyl acrylate) nanocomposites and evaluating the effect of these nanoplatelets on the kinetics of copolymerization and thermal properties of the products. General procedure for the synthesis of tailor-made random poly(styrene-co-butyl acrylate) chains via normal ATRP in the presence of the pristine diatomite nanoplatelets is illustrated in Fig. 6.

Number and weight average molecular weights, dispersity, and effect of the pristine diatomite nanoplatelets on these parameters is evaluated by SEC analysis. Figure 7 presents SEC traces of the samples. According to the Fig. 7, SEC traces of the neat poly(styrene-co-butyl acrylate) and all of the nanocomposites display monomodal peaks corresponding to the molecular weight values predetermined by the molar ratio of monomer to initiator. Pure poly(styrene-co-butyl acrylate) reveals narrow distribution and low dispersity value which can demonstrate successful normal ATRP is established.

Normal ATRP of styrene and butyl acrylate without diatomite nanoplatelets results in well-defined poly(styrene-co-butyl acrylate) chains with low dispersity value. By adding the pristine diatomite nanoplatelets, final conversion and molecular weight were increased. By addition of only 3 wt% of the pristine diatomite nanoplatelets, final conversion increases from 65 to 78%. Extracted data from SEC traces of the neat poly(styrene-co-butyl acrylate) and its different nanocomposites are summarized in Table 2.

Theoretical molecular weight is calculated by using Eq. 1:

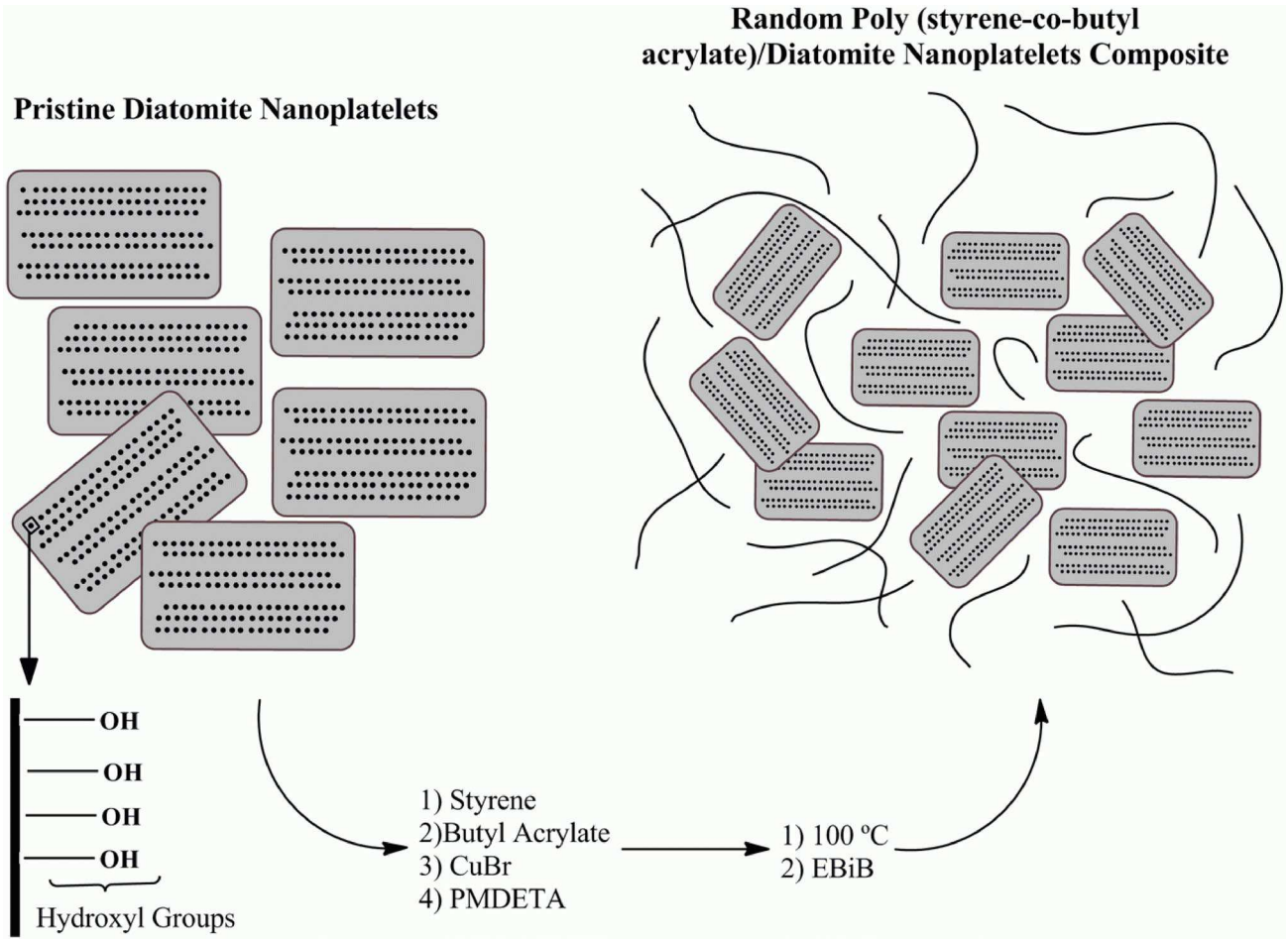

Fig. 6 General procedure for the synthesis of poly(styrene-co-butyl acrylate)/diatomite nanocomposites via normal ATRP

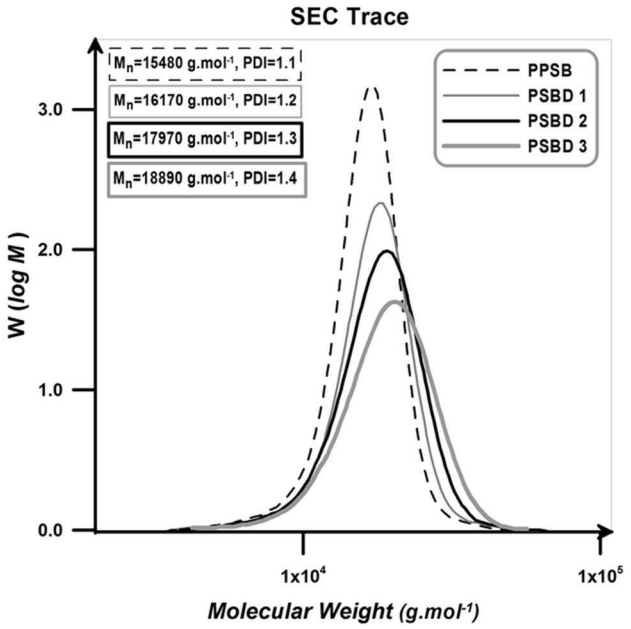

Fig. 7 SEC traces of the neat poly(styrene-co-butyl acrylate) and its different nanocomposites

$$M_n^{Theo} = \frac{[M]_0}{[I]_0} \times p \times Mw \quad (1)$$

where, $[M]_0$ and $[I]_0$ are initial concentration of the monomers and initiator, respectively. Conversion is denoted by p and the symbol of the average molecular weight of the monomers is Mw.

Positive effect of the pristine diatomite nanoplatelets on the molecular weight of the samples can be interpreted by abundant pendant hydroxyl groups of the pristine diatomite. It is demonstrated that polar solvents (especially hydroxyl containing ones like water, phenol, and carboxylic acids) exert a rate acceleration effect on the polymerization systems for increasing radical activation rate and also reducing radical recombination rate [41–43]. Pendant hydroxyl groups on the surface of the pristine diatomite can possibly cause a polarity change into the reaction medium. In addition, negatively charged surface (pendant hydroxyl groups on the surface of the pristine diatomite at our work) could absorb and gather positively charged catalyst (Cu ions at this work) [44, 45]. By

Table 2 Molecular weights and PDI values of the extracted copolymers resulted from SEC traces

Sample	Reaction time (h)	Conversion (%)	M_n		PDI
			Exp.	Theo.	
PPSB	12	65	1.1	15,101	15,500
PSBD 1	12	71	1.2	16,495	16,000
PSBD 2	12	74	1.3	17,192	18,000
PSBD 13	12	78	1.4	18,121	19,000

adsorbing the catalyst particles, the ATRP equilibrium will be affected and chain growth rate can be enhanced [41, 46]. The accelerating effect of other nano-fillers such as nanoclay and MCM-41 nanoparticles on (co)polymerization rate was also reported elsewhere [41–43]. Dispersity values of the copolymer chains increases by the addition of pristine diatomite loading. Pristine diatomite nanoplatelets act as an impurity in the copolymerization medium and therefore cause the molecular weight distribution of the resultant copolymers to be increased; dispersity value increases from 1.1 to 1.4 by 3 wt% loading of pristine diatomite [47, 48].

An appropriate agreement between the theoretical and experimental molecular weights in combination with low dispersity values (dispersity <1.4) can be considered as an appropriate evidence for controlled nature of the copolymerization (Table 2). Also, color change of the reaction media from light green to light brown during the copolymerization is an evidence of successful ATRP equilibrium establishment.

Composition of the copolymer chains are evaluated by ^{1}H NMR spectroscopy. Figure 8 represents ^{1}H NMR spectra of the neat poly(styrene-co-butyl acrylate) and its various nanocomposites.

Molar ratio of each monomer in the copolymer chains can be determined by integrating aromatic peaks area (S_{Ph}, 6.6–7.4 ppm, 5H) which corresponds to the phenyl ring of styrene and methylene near to the ester group of butyl acrylate (S_M, 3.6–4.2 ppm, 2H) by using Eqs. (2) and (3):

$$\%St = \frac{\frac{A_{Ph}}{5}}{\left(\frac{A_{Ph}}{5} + \frac{A_M}{2}\right)} \times 100 \quad (2)$$

$$\%BA = \frac{\frac{A_M}{2}}{\left(\frac{A_{Ph}}{5} + \frac{A_M}{2}\right)} \times 100 \quad (3)$$

According to the results (Fig. 8), molar ratio of each monomer in all the samples is approximately similar to the initial selected mole ratio of the monomers.

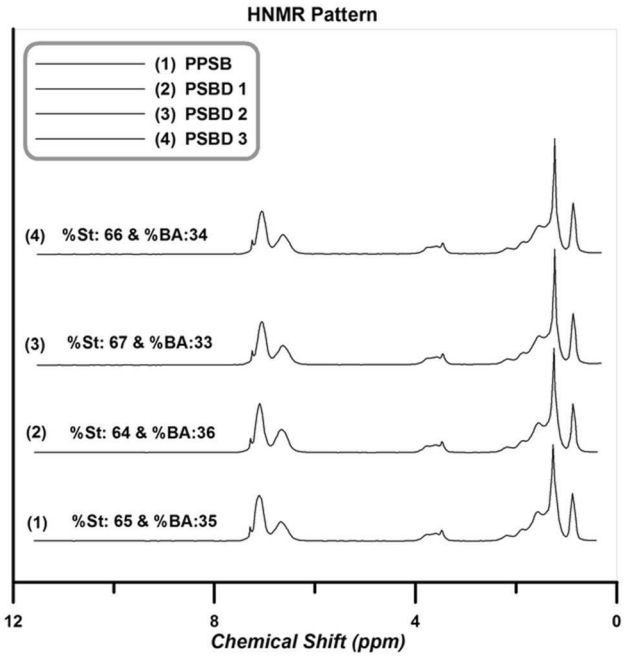

Fig. 8 ^{1}H NMR spectra of the neat poly(styrene-co-butyl acrylate) and its different nanocomposites

TGA was used to study thermal stability of the neat poly(styrene-co-butyl acrylate) and its various nanocomposites. TGA thermograms of weight loss as a function of temperature in the temperature window of 30–700 °C are shown in Fig. 9.

According to the Fig. 9, thermal stability of the neat poly(styrene-co-butyl acrylate) is lower than all of the nanocomposites. In addition, thermal stability of the neat poly(styrene-co-butyl acrylate) is improved by adding

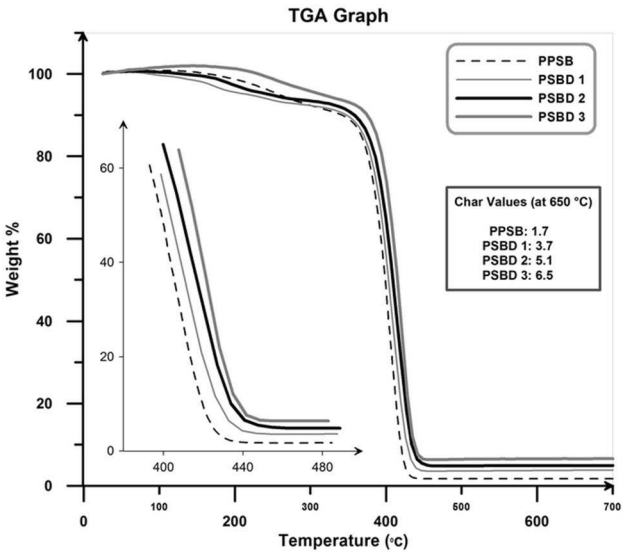

Fig. 9 TGA thermograms of the neat poly(styrene-co-butyl acrylate) and its nanocomposites

pristine diatomite nanoplatelets which by increasing diatomite content, an increase in degradation temperatures was observed. In general, by increasing temperature in the TGA graphs three separated steps can be identified: evaporation of the water molecules (at the temperature range of 100–150 °C), degradation of volatile materials such as residual monomer and low molecular weight oligomers (at the temperature window around 180–350 °C), and degradation of the synthesized copolymer and nanocomposites (at the temperatures above 380 °C). Figure 10 graphically illustrates the extracted data from TGA graphs. Degradation temperature of the samples versus amount of degradation is employed to show that addition of diatomite in the poly(styrene-co-butyl acrylate) matrix, results in an improvement of thermal stabilities of the nanocomposites (T_X: temperature threshold at which X% of neat poly(styrene-co-butyl acrylate) and its nanocomposites is degraded).

Increasing of degradation temperature of the nanocomposites by adding pristine diatomite nanoplatelets content is attributed to the high thermal stability of diatomite nanoplatelets and also interaction between diatomite nanoplatelets and copolymer matrix [49]. Physical interaction between poly(styrene-co-butyl acrylate) chains and surface of the pristine diatomite nanoplatelets is an important factor for increasing thermal stability of the nanocomposites [50]. Additionally, hindrance effect of the pristine diatomite platelets on the copolymer chains movement and restriction of oxygen permeation by these sheets are the other reasons for higher thermal stability of the nanocomposites. Similar conclusions are also achieved in the case of polymer/clay nanocomposites [43, 51].

DSC analysis is employed to evaluate the effect of pristine diatomite nanoplatelets on the chain confinement of the samples and determination of glass transition temperature (T_g). Figure 11 displays DSC thermograms of the neat poly(styrene-co-butyl acrylate) and its different nanocomposites. Temperature range of 20–170 °C is used to describe DSC results in the heating path. Pristine diatomite nanoplatelets do not bear any transitions in this range of temperature, therefore only thermal transition of copolymers is observed. In these experiments, samples are heated from room temperature to 225 °C to remove their thermal history. Then, they cooled to room temperature to distinguish the phase conversion and other irreversible thermal behaviors. Finally, samples are heated from room temperature to 225 °C to obtain T_g values.

According to the Fig. 11, an obvious inflection takes place in the temperature range of 30–40 °C in which shows T_g of the samples. Since there is not another peak in the cooling path (except T_g), amorphous structure of the samples can be concluded.

According to the results, T_g value of the neat poly(styrene-co-butyl acrylate) is lower than all of the nanocomposites and an increase in T_g values takes place by increasing of pristine diatomite nanoplatelets content. Increasing T_g values by adding pristine diatomite nanoplatelets loading in the copolymer matrix can be attributed to the confinement effect of the diatomite platelets. The rigid two-dimensional diatomite platelets can restrict the steric mobility of copolymer chains and causes the inflection in the DSC graphs starts at higher temperatures.

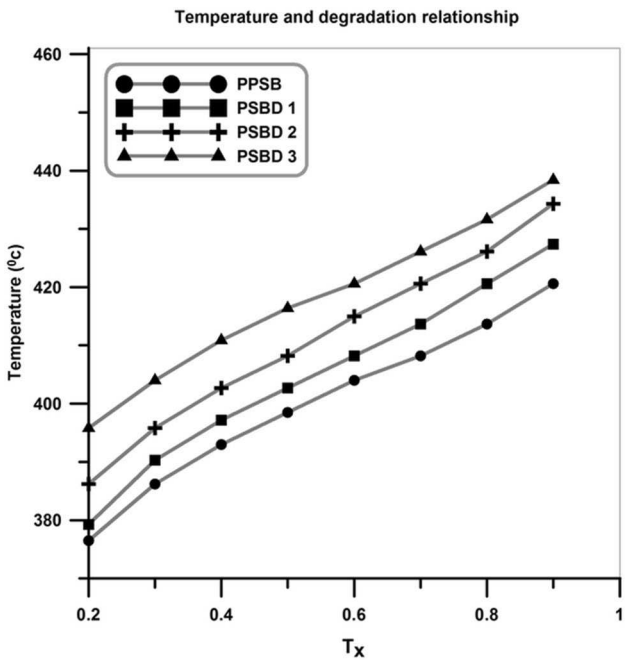

Fig. 10 Graphical illustration of temperature and degradation relationship

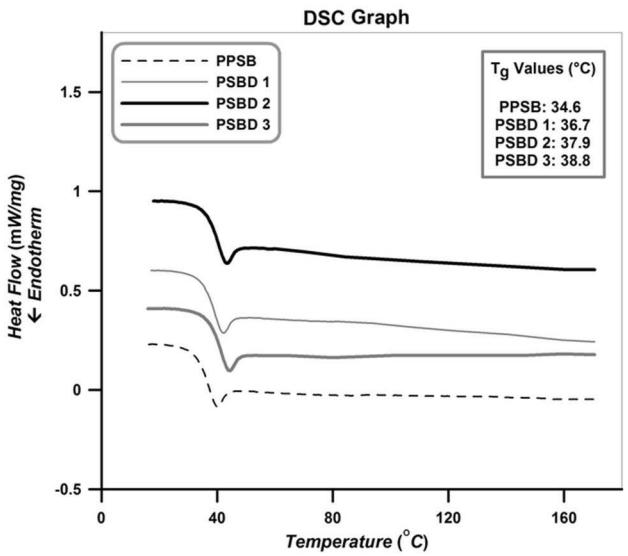

Fig. 11 DSC thermograms of the neat poly(styrene-co-butyl acrylate) and its different nanocomposites (heating path)

Similar conclusions are also obtained in the case of polymer/clay nanocomposites [43, 51, 52].

4 Conclusions

In situ atom transfer radical random copolymerization of styrene and butyl acrylate was employed to synthesize tailor-made random poly(styrene-co-butyl acrylate) and its different nanocomposites in the presence of pristine mesoporous diatomite platelets. Porous structure, existence of plaque plate particles with spherical pores, silica as the main constituent, and existence of numerous regularly spaced rows in its structure are some inherent features of the pristine diatomite nanoplatelets. In situ ATRP of styrene and butyl acrylate in the presence of pristine mesoporous diatomite leads to increment of conversion from 65 to 78%. Moreover, molecular weight and dispersity values increase from 15,500 to 19,000 and from 1.1 to 1.4 respectively. ^{1}H NMR spectroscopy results show that copolymers composition is approximately similar to the initial feed ratio of each monomer. Improvement in thermal stability of the nanocomposites and increasing T_g values from 34.6 to 38.8 °C was also observed by incorporation of 3 wt% of pristine mesoporous diatomite platelets.

References

1. S. Bhattacharya, S.K. Samanta, Chem. Rev. (2016). doi:10.1021/acs.chemrev.6b00221
2. H. Roghani-Mamaqani, K. Khezri, Appl. Surf. Sci. **360**, 373 (2016)
3. A. R. Gangopadhyay De, Chem. Mater. **12**, 608 (2000)
4. S.L. Burkett, N. Ko, N.D. Stern, J.A. Caissie, D. Sengupta, Chem. Mater. **18**, 5137 (2006)
5. F. Hussain, M. Hojjati, M. Okamoto, R.E. Gorga, J. Compos. Mater. **40**, 1511 (2006)
6. R.P. Singh,, A. Tiwari, A.C. Pandey, J. Inorg. Org. Polym. Mater. **21**, 788 (2011)
7. M. Zanetti, S. Lomakin, G. Camino, Macromol. Mater. Eng. **279**, 1 (2000)
8. S. Varghese, J. Karger-Kocsis, Polymer **44**, 4921 (2003)
9. S. Nenadovic, M. Nenadovic, R. Kovacevic, Lj. Matovic, B. Matovic, Z. Jovanovic, J. Grbovic Novakovic, Sci. Sinter. **41**, 309 (2009)
10. Y. Jia, W. Han, G. Xiong, W. Yang, Sci. Technol. Adv. Mater. **8**, 106 (2007)
11. W-T. Tsai, C-W. Lai, K-J. Hsien, J. Coll. Interface Sci. **297**, 749 (2006)
12. S. Akin, J.M. Schembre, S.K. Bhat, A.R. Kovscek, J. Petrol. Sci. Eng. **25**, 149 (2000)
13. Y.S. Al-Degs, M.F. Tutunju, R.A. Shawabkeh, Sep. Sci. Technol. **35**, 2299 (2000)
14. N. Caliskan, A.R. Kul, S. Alkan, E.G. Sogut, I. Alacabey, J. Hazard. Mater. **193**, 27 (2011)
15. I. Ruggiero, M. Terracciano, N. M. Martucci, L. De Stefano, N. Migliaccio, R. Tatè, I. Rendina, P. Arcari, A. Lamberti, I. Rea, Nanoscale Res. Lett. **9**, 329 (2014)
16. K. Khezri, V. Haddadi-Asl, H. Roghani-Mamaqani, M. Salami-Kalajahi, J. Polym. Res. **19**, 9868 (2012)
17. P.B. Zetterlund, Y. Kagawa, M. Okubo, Chem. Rev. **108**, 3747 (2008)
18. E. Mastan, X. Li, S. Zhu, Prog. Polym. Sci. **45**, 71 (2015)
19. X. Pan, M.A. Tasdelen, J. Laun, T. Junk, Y. ers, Yagci, K. Matyjaszewski, Prog. Polym. Sci. (2016). doi: 10.1016/j.progpolymsci.2016.06.005
20. S. Beyazit, B.T. Sum Bui, K. Haupt, C. Gonzato, Prog. Polym. Sci. (2016). doi: 10.1016/j.progpolymsci.2016.04.001
21. G. Moad, E. Rizzardo, S.H. Thang, Aust. J. Chem. **59**, 669 (2006)
22. K. Matyjaszewski, J. Xia, Chem. Rev. **101**, 2921 (2001)
23. J. Nicolas, Y. Guillaneuf, C. Lefay, D. Bertin, D. Gigmes, B. Charleuxc, Prog. Polym. Sci. **38**, 63 (2013)
24. J. Ran, L. Wu, Z. Zhang, T. Xu, Prog. Polym. Sci. **39**, 124 (2014)
25. V. Coessens, T. Pintauer, K. Matyjaszewski, Prog. Polym. Sci. **26**, 337 (2001)
26. V. Kuppa, E. Manias, Chem. Mater. **14**, 2171 (2002)
27. S. Karaman, A. Karaipekli, A. Sarı, A. Bicer, Solar Energy Mater. Solar Cells **95**, 1647 (2011)
28. X. Li, C. Bian, W. Chen, J. He, Z. Wang, N. Xu, G. Xue, Appl. Surf. Sci. **207**, 378 (2003)
29. X. Li, X. Li, G. Wang, Appl. Surf. Sci. **249**, 266 (2005)
30. S. Hu, X. Zhu, W. Hu, L. Yan, C. Cai, Polym. Bull. **70**, 517 (2013)
31. J.Z. Liang, Polym. Test. **27**, 936 (2008)
32. H. Roghani-Mamaqani, K. Khezri, J. Polym. Res. **23**, 190 (2016)
33. G. Sheng, H. Dong, Y. Li, J. Environ. Radioact. **113**, 108 (2012)
34. P. Yuan, D. Liu, D. Tan, K. Liu, H. Yu, Y. Zhong, A. Yuan, W. Yu, H. He, Microporous Mesoporous Mater. **170**, 9 (2013)
35. Y. Yu, J. Addai-Mensah, D. Losic, Sci. Technol. Adv. Mater. **13**, 015008 (2012)
36. K. Khezri, RSC Adv. **6**, 109286 (2016)
37. N. Garderen, F.J. Clemens, M. Mezzomo, C.P. Bergmann, T. Graule, Appl. Clay Sci. **52**, 115 (2011)
38. Y. Du, J. Yan, Q. Meng, J. Wang, H. Dai, Chem. Phys. **133**, 907 (2012)
39. Z. Sun, X. Yang, G. Zhang, S. Zheng, R.L. Frost, Int. J. Miner. Process. **125**, 18 (2013)
40. Y. Fazli, K. Khezri, H. Alijani, Adv. Polym. Technol. **35**, 21549 (2016)
41. D. Liu, P. Yuan,, D. Tan, H. Liu, T. Wang, M. Fan, J. Zhu, H. He, J. Coll. Interf. Sci. **388**, 176 (2012)
42. A. Asfadeh, V. Haddadi-Asl, M. Salami-Kalajahi, M. Sarsabili, H. Roghani-Mamaqani, Nano **8**, 1350018 (2013)
43. H. Roghani-Mamaqani, V. Haddadi-Asl, M. Najafi, M. Salami-Kalajahi, J. Appl. Polym. Sci. **120**, 1431 (2011)
44. C. Wu, X. Xu, J. Liang, Q. Wang, Q. Dong, W. Liang, Desalination **279**, 140 (2011)
45. G. Sheng, S. Wang, J. Hu, Y. Lu, J. Li, Y. Dong, X. Wang, Coll. Surf. A. **339**, 159 (2009)
46. J.N. Kizhakkedathu, D.E. Brooks, Macromolecules **36**, 591 (2003)
47. H. Roghani-Mamaqani, V. Haddadi-Asl, M. Najafi, M. Salami-Kalajahi, J. Appl. Polym. Sci. **123**, 409 (2012)
48. M. Salami-Kalajahi, V. Haddadi-Asl, S. Rahimi-Razin, F. Behboodi-Sadabad, M. Najafi, H. Roghani-Mamaqani, J. Polym. Res. **19**, 9793 (2012)
49. S. Subramania, S.W. Choia, J.Y. Lee, J.H. Kim, Polymer **48**, 4691 (2007)
50. M.A. Ver Meer, B. Narasimhan, B.H. Shanks, S.K. Mallapragada, ACS Appl. Mater. Interfaces **2**, 41 (2010)
51. Y. Fazli, E. Kulani, K. Khezri, H. Alijani, Micropor. Mesopor. Mater. **214**, 70 (2015)
52. M. Sarsabili, K. Kalantari, K. Khezri, J. Therm. Anal. Calorim. **126**, 1261–1272 (2016)